Quantitative detection of chemical compounds in human hair with coherent anti-Stokes Raman scattering microscopy

Maxwell Zimmerley
Chia-Yu Lin
University of California, Irvine
Department of Chemistry
Irvine, California 92697

David C. Oertel
Jennifer M. Marsh
The Procter & Gamble Company
11810 East Miami River Road
Cincinnati, Ohio 45252

Jimmie L. Ward
The Procter & Gamble Company
11510 Reed Hartman Highway
Cincinnati, Ohio 45252

Eric Olaf Potma
University of California, Irvine
Department of Chemistry
Irvine, California 92697
E-mail: epotma@uci.edu

Abstract. Coherent anti-Stokes Raman scattering (CARS) microscopy is used to determine the distribution and concentration of selected compounds in intact human hair. By generating images based on ratiometric CARS contrast, quantitative concentration maps of both water and externally applied d-glycine are produced in the cortex of human hair fibers. Both water and d-glycine are found to homogeneously distribute throughout the cortical regions of the hair. The ability to selectively detect molecular agents in hair fibers is of direct relevance to understanding the chemical and physical mechanisms that underlie the performance of hair-care products. [DOI: 10.1117/1.3184444]

Keywords: medical imaging; molecular spectroscopy; multiphoton process; Raman spectroscopy; water.

Paper 09097R received Mar. 20, 2009; revised manuscript received Jun. 2, 2009; accepted for publication Jun. 2, 2009; published online Aug. 5, 2009.

1 Introduction

The penetration of small molecules into human hair fibers is a process of significant interest to the personal care and cosmetic industry. For hair-care products, such as shampoos and conditioners, the successful penetration of these small molecules can impact the internal structure of the hair and ultimately hair properties, such as tensile strength.[1] For hair-color products the penetration of the dye precursors and oxidants into the hair is crucial for the achievement of the desired color.[2] Thus, the ability to measure factors such as penetration depth, distribution pattern in the fiber, and local concentration of the molecular agent can give important insight into the ultimate performance of the hair-care and hair-color products. These measures also serve as essential parameters in studying the underlying chemical and physical mechanisms that govern the interaction of hair-care products with the hair fiber.

Electron microscopy techniques have been instrumental in understanding the fine structure of both the surface as well as the interior of the hair.[3,4] The high resolution offered by scanning electron microscopy (SEM) renders this technique ideal for observing morphological changes in the hair fiber as induced by chemical agents. Similarly, optical microscopy tools, though at a lower spatial resolution relative to SEM, have been used for inspecting the morphology of both the surface and interior of the hair.[5,6] Although morphology studies are highly instructive, this technique does not easily allow for the visualization of a penetrating agent inside the hair.

Chemically selective detection of molecular agents in the hair has been achieved using techniques such as autoradiography[7] and micro X-ray fluorescence analysis in combination with high-resolution SEM.[8] Although such probing techniques are useful for determining the location of certain chemicals in the hair, they require sample preparation methods that can compromise the three-dimensional structure of the hair, obscuring a direct correlation between the distribution of the chemical and the morphology of the hair.

Optical methods, on the other hand, allow for nondestructive probing of chemical structures in the hair. High-resolution optical microscopy techniques, including near-field optical microscopy, have been employed to determine the pathways of externally applied molecules through the hair.[9] Nonetheless, optical studies thus far have been limited to following the diffusion of fluorescent dye molecules in hair fibers.[9,10] Consequently, the detection of nonfluorescent substances in the intact hair remains a challenge.

The use of vibrational microscopy circumvents the use of fluorescent probes and offers an avenue for directly detecting the uptake of various molecules by human hair fibers without the complications of significant sample preparation. Infrared microscopy has been successfully applied to record the chemical changes within the hair before and after bleaching.[11] However, such an approach is less attractive when submicron

Address all correspondence to: Eric Olaf Potma, University of California, Irvine, Department of Chemistry, Irvine, CA 92697; E-mail: epotma@uci.edu

1083-3668/2009/14(4)/044019/7/$25.00 © 2009 SPIE

resolution is required, or when rapid image acquisition is desired for monitoring the penetration of the agent dynamically. Similarly, Raman microscopy has been used to characterize endogenous components of the hair. Whereas Raman microspectroscopy has been useful for chemical analysis in selected locations in the hair,[12] it has been less successful in providing high-resolution concentration maps of compounds of interest because of the inherently long signal integration times.

In this work, we use an alternative vibrational imaging method, coherent anti-Stokes Raman scattering (CARS) microscopy, for registering the distribution of molecular agents in human hair. CARS microscopy is a nondestructive optical imaging technique that enables high-resolution three-dimensional imaging at real-time image acquisition rates.[13,14] We show that the CARS approach provides a direct means of quantitatively probing the distribution and concentration of nonfluorsscent compounds in the hair.

Nonlinear vibrational imaging, which includes CARS microscopy and stimulated Raman scattering microscopy,[15] has been successfully applied to a wide variety of biomedical imaging problems, including applications in neurological[16] and cardiovascular disease.[17] In many tissue imaging studies, it is often sufficient to qualitatively identify particular compounds and structures based on visual inspection of the vibrational images. Quantitative mapping of the molecular concentration is challenging because of tissue scattering, which directly affects the collected signal intensity and thus complicates a quantitative analysis. Scattering is particularly relevant to optical imaging of hair fibers, given that the refractive index of hair fibers is typically much higher than that of the surrounding medium. A direct analysis is furthermore compromised because scattering is not uniform across the radius of cylindrical hair fibers. In addition, in CARS, the signal depends in a nonlinear fashion on the concentration of the Raman scatterers.

In this paper, we use a simple ratiometric procedure to retrieve quantitative information from CARS images. This procedure is used to generate concentration maps of two molecular agents, water and deuterated (d-)glycine, that are externally applied to the hair. The ability to record water concentration maps in the hair is of significant interest because how the hair responds to different levels of hydration (i.e., under different humidity conditions) impacts many cosmetic properties, such as frizz and style retention.[18] It is also present in hair at relatively high levels (10–30% of the hair's weight). Glycine was chosen as the second molecular agent to study using this technique because the concentration in hair is much lower than water and would demonstrate the ability of the technique to measure the penetration of cosmetic actives into hair. Glycine is of relevance to the cosmetics industry due to its reported role as a radical scavenger in a new oxidant system developed for hair-coloring products.[19] Knowledge of the actual distribution of glycine in the hair is important for better assessing the chemistry during the coloring process.

We demonstrate that CARS microscopy enables the quantitative detection of both water and deuterated glycine, a weak Raman scatterer, in intact human hair fibers. The technique has also demonstrated the ability to monitor the dynamic uptake of water into hair enabling new insights into the kinetics of diffusion.

2 Materials and Methods

2.1 *Materials*

Caucasian untreated natural white hair, obtained from a commercial source (International Hair Importers, New York), was formed into swatches (16 cm, 1.5 g). White hair was chosen to avoid putative photodamage induced by linear absorption of the laser light by melanin. The hair was cut into ~1-cm segments and mounted on a glass coverslip using double-sided adhesive sheets (Grace Biolab). Because glass has no resonances in the spectral region of interest, a small coverslip (~170 μm thick) was placed next to the hair to serve as an internal calibration for normalizing the CARS signal. D_2O and d-glycine (d5) were obtained from Sigma-Aldrich. In this study, d-glycine is used as a model for glycine because of the enhanced CARS contrast of provided by the deuterium label.

In the d-glycine uptake experiments, the hair was immersed for at least 4 h in an aqueous solution of 3.3 M d-glycine and 0.52 M ammonium carbonate, adjusted to pH 9.0 for efficient uptake into the hair.[19] The hair was kept in the solution during the imaging experiments.

2.2 *Imaging*

A 76-MHz mode-locked laser source (PicoTrain, High-Q Lasers), which produced 7-ps-pulsed 1064-nm light, was used as the Stokes beam in the CARS process. The source also produces a frequency-doubled, 532-nm beam, which was used to pump a picosecond optical parametric oscillator [(OPO), Levante Emerald]. The OPO delivers radiation tunable in the 650–970 nm range, which was employed as the pump beam in the CARS process. The two beams were collinearly overlapped on a dichroic mirror and directed to a galvanometric scanner (Fluoview 300V, Olympus) before entering an inverted microscope (IX-71, Olympus). A 40×, NA 1.15 water-immersion objective lens (UplanApo, Olympus) was utilized in these studies. Average illumination dose was 15 mW per beam. The forward-propagating CARS signal was collimated by a 0.55-NA condenser, passed through two bandpass filters, and detected by a red-sensitive photomultiplier tube [R3896, Hamamatsu]. All images (512×512 pixels) were collected in 1.5 s per frame and averaged three times. CARS spectra were obtained by scanning the OPO wavelength while keeping the 1064-nm Stokes beam fixed. All CARS signals were normalized relative to the nonresonant signal from a glass coverslip.

2.3 *Image Processing*

To convert the CARS intensity images to concentration maps, we have employed the enhanced contrast obtained when using ratio images. For a given vibrational band, ratio images between the maximum CARS signal and the minimum CARS signal were generated. Because of the dispersive line shape of CARS spectral features, the resonance peak was taken as the maximum and the dip on the blue side of the Raman resonance frequency was chosen as the minimum CARS signal. Ratio images were constructed in the following way. (*i*) An image was taken at the CARS spectral maximum, followed by a background reference image obtained by blocking the Stokes beam. (*ii*) An image at the CARS spectral minimum was recorded, and supplemented with a background reference

image. (*iii*) The backgrounds were subtracted from the maximum and minimum CARS images. (*iv*) The resulting images were corrected for the intensity dependence of the field of view by dividing each by a prerecorded CARS field-of-view intensity profile. The field-of-view correction profile was obtained for each spectral setting and obtained by recording a field profile of the nonresonant signal of the supporting glass coverslip. Each correction profile was corrected for any background contributions. (*v*) The CARS ratio image was obtained by dividing the maximum by the minimum image. Because all ratio images are scaled relative to the nonresonant glass signal, a direct quantitative comparison between the processed images is possible. All image processing was performed within the ImageJ environment,[20] using home-written software. The total processing time for generating a calibrated concentration map is <1 min.

2.4 *Concentration Dependence*

At low concentrations of the Raman scatterer, the ratiometric CARS signal is more sensitive than the regular CARS intensity to changes in the concentration. CARS imaging based on a comparison of signals measured at different Raman shifts is a common procedure for improving the image contrast.[21,22] The ratio signal employed here enhances the contrast obtained from small concentration differences. Under the assumption that the nonresonant electronic contribution is invariant among the sample components, the ratiometric signal $R(c)$ can be written as

$$R(c) = \frac{1 + c^2|A(\omega_+)|^2 + 2c \cdot \mathrm{Re}\{A(\omega_+)\}}{1 + c^2|A(\omega_-)|^2 + 2c \cdot \mathrm{Re}\{A(\omega_-)\}}, \quad (1)$$

where c is the concentration, $\omega_{+/-}$ is the vibrational frequency at the chosen maximum and minimum of the CARS signal, and $A(\omega)$ is the complex spectral bandshape function, normalized to the nonresonant background. It is instructive to examine the behavior of $R(c)$ in several important limits, assuming a single Lorentzian-shaped band profile. When the vibrational contribution is weak, i.e., $c^2|A(\omega_+)|^2 \ll 1$ and $\mathrm{Re}\{A(\omega_-)\} = -\mathrm{Re}\{A(\omega_+)\}$, the ratiometric signal can be written as

$$R(c) \approx \frac{1 + 2c \cdot \mathrm{Re}\{A(\omega_+)\}}{1 - 2c \cdot \mathrm{Re}\{A(\omega_+)\}} \approx 1 + 4c \cdot \mathrm{Re}\{A(\omega_+)\}. \quad (2)$$

For weak Raman scatterers, we thus expect a linear concentration dependence. With a stronger vibrational contribution, $R(c)$ grows increasingly more nonlinear. For very strong vibrational resonances ($c^2|A(\omega_+)|^2 \gg 1$), $R(c)$ reaches a maximum and eventually decreases at higher concentrations. The use of $R(c)$ as a contrast parameter is therefore most useful when applied to determine the concentration of relatively weak Raman scatterers. We use the $R(c)$ calibration curve as an empirical link between the ratiometric signal and the actual concentration of the Raman scatterer.

Concentration maps were determined by converting the ratio scale to a concentration scale using a calibration graph. For both water and d-glycine, the maximum and minimum CARS signal was obtained as a function of the concentration of the target compound. A calibration curve was acquired by plotting the corrected CARS ratio between the maximum and minimum against concentration. A polynomial fit was used to describe the concentration dependence of $R(c)$. Note that the glass-normalized CARS ratio is always independent of such factors as image-to-image laser intensity variation, which enables a direct conversion from CARS ratio images to concentration with the aid of the ratiometric calibration curve.

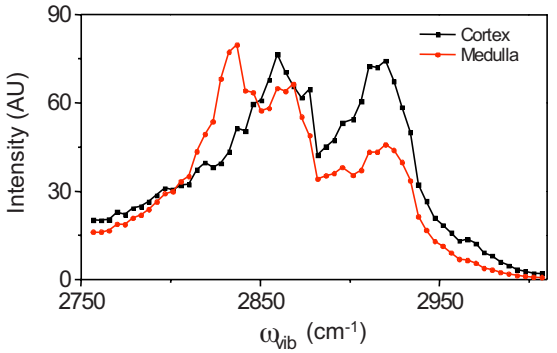

Fig. 1 CARS spectrum of the cortex (black dots) and the medulla (red dots) of human hair. The CH_2-symmetric stretch (2840 cm^{-1}) indicates the presence of lipids in the medulla, whereas the cortex is rich in CH_3-symmetric stretch (2920 cm^{-1}) associated with keratin structural proteins. (Color online only.)

3 Results

3.1 *CARS Microscopy of Endogenous Hair Components*

Before studying the concentration of externally applied compounds to the hair, we first examined the CARS response of several major endogenous components of the hair. The CARS spectrum of D_2O-immersed hair measured in both the cortex and medulla is given in Fig. 1. Relative to a dry hair, immersion in D_2O leads to a better refractive index match between the slide and sample. The D_2O was chosen because it is minimally vibrationally resonant in the 2800–3000 cm^{-1} range, the spectral region of the CH_2- and CH_3-stretching vibrational modes.

As is evident from Fig. 1, the spectra of the cortex and the medulla are different. In the medulla, a higher contribution from the symmetric CH_2 stretching mode (2840 cm^{-1}) is observed, an indication of a higher density of lipid aliphatic chains. A higher relative lipid concentration in the medulla was also observed in infrared microspectroscopy studies.[23] Importantly, compared to infrared microscopy techniques, the higher resolution in CARS allows for a much finer assessment of the distribution of lipids in the medulla. It is seen in Fig. 2 that the lipids are nonhomogeneously distributed. The lipid clusters resemble the globular structures previously observed with SEM.[4] The spectral profile of the cortex mimics the CARS spectrum of structural proteins.[24] This is an expected result, as the density of keratin in the cortex is higher than in the porous area of the medulla.

3.2 *Water Concentration in the Hydrated Hair*

The vibrational sensitivity of CARS permits the registration of externally applied compounds in the hair. To visualize water, the OH-stretching vibrational range is used for generating contrast. The CARS spectrum of water is depicted in Fig. 3,

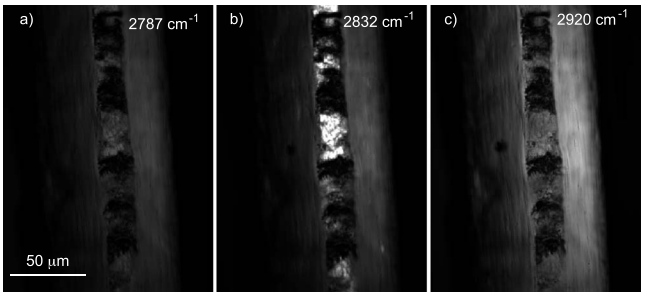

Fig. 2 CARS images of human hair at different Raman shifts. Images were taken at the equatorial plane of the hair: (a) nonresonant background contribution from both cortex and medulla at 2787 cm^{-1}, (b) lipid contrast of the CH_2-symmetric stretch probed at 2832 cm^{-1}. Note that the medulla exhibits lipid rich areas not seen in the cortex, and (c) protein contrast based on the CH_3 symmetric stretch at 2920 cm^{-1}. A strong signal from the keratin-dense cortex is observed.

showing the broad band of the OH-stretching vibrations. To quantitatively analyze the distribution of water within the hair, ratio images of the hydrated hair were constructed by taking images at 3100 and 3550 cm^{-1}. Note that both vibrational energies exhibit minimum overlap with the Raman vibrational energies of the hair's endogenous components. A calibration curve was generated by using solutions of varying H_2O/D_2O ratios to record the dependence of the ratio signal as a function of H_2O volume percent. In determining the calibration curve, we have ignored the subtle spectral changes as a consequence of HOD formation. The calibration curve for the ratio signal ratio is depicted in Fig. 4. The concentration dependence of the ratiometric signal exhibits a smooth profile and is well described by the polynomial fitting function plotted in Fig. 4.

In Fig. 5(a), the water concentration map of a hair immersed in water is shown. The water concentration in the hair is homogenously distributed, and the spatially averaged concentration was found to be 34% by volume. At full hydration, hair can absorb ~30% of its dry weight in water.[18] The density of dry hair is ~1.32 g/cm^3, and the hair can absorb ~0.40 g/cm^3 of water.[2] Assuming a 30% volume increase of

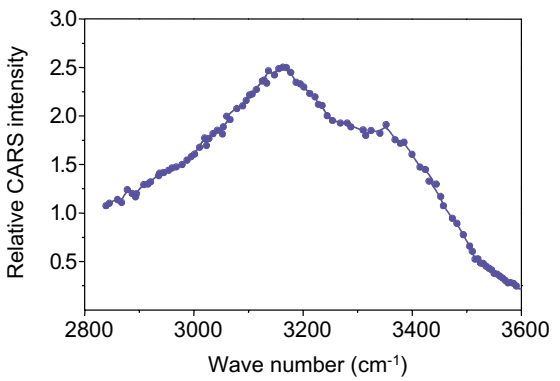

Fig. 3 CARS spectrum of water in the OH-stretching region. The CARS signal is measured relative to the nonresonant response from a glass coverslip. The signal around 3100 cm^{-1} is taken as the maximum and the dip at 3550 cm^{-1} is taken as the minimum in the CARS ratio images for water.

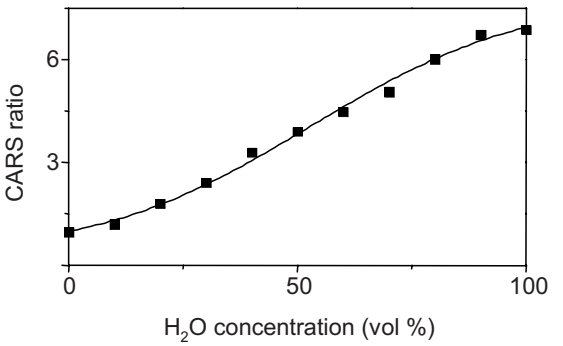

Fig. 4 Dependence of the CARS ratio signal as a function of water volume concentration in a $H_2O:D_2O$ mixture. The data points are fitted to a polynomial.

the fully hydrated hair,[25] the maximum water concentration in the hair amounts to ~31 vol %, which is in close agreement with the water concentration found in the CARS measurement.

Note that in the ratio images, the signal-to-noise near the boundary of the hair is rather low, due to the fact that at the hair/water interface the CARS signal is severely reduced as a consequence of light scattering. Nonetheless, while the signal from these regions cannot be used for a quantitative analysis, they provide a clear demarcation of the hair's surface. To facilitate the analysis, we have chosen a hair that is devoid of a highly scattering medulla. As a control, the water concentration in a hair immersed in pure D_2O was determined. The ratio image of the D_2O-immersed hair is shown in Fig. 5(b). As expected, no significant ratiometric contrast was observed under these conditions, which illustrates the feasibility of the CARS ratio images as a probe for water concentration.

3.3 *Dynamic Water Uptake*

When hair fibers are fully hydrated in pure water, a significant swelling of up to ~30% can be observed.[26] It is, however, unclear whether the swelling of the hair is linearly dependent on the absorbed water concentration or whether other dynamic structural changes during the hydration process are re-

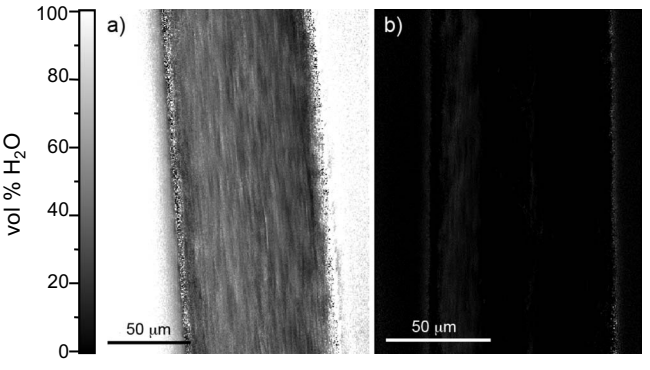

Fig. 5 Water concentration maps determined from CARS ratiometric images (3100 cm^{-1}/3550 cm^{-1}) at the OH-stretching vibration: (a) water concentration in a hair immersed in pure H_2O and (b) water concentration in a hair immersed in pure D_2O. The lack of contrast in the D_2O image indicates that the ratiometric contrast of the hair itself is negligible.

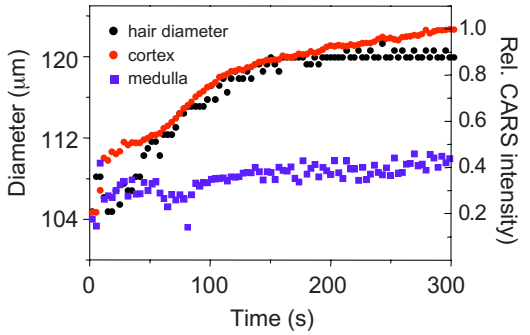

Fig. 6 Dynamic recording of the relative CARS signal at 3100 cm^{-1} as a function of time after immersion of hair in water. Black dots indicate the change of the hair diameter, red dots the temporal dependence of the relative CARS signal in the cortex, and the blue squares the gradual increase of the CARS signal in the medulla. (Color online only.)

sponsible for the increased diameter of the hair. Because of the fast imaging capability of the CARS microscope, a direct correlation between swelling and intrahair water concentration can be obtained.

We have performed dynamic water measurements in hair by probing the CARS water signal at 3100 cm^{-1} during the immersion of a dry hair in pure water. Representative results are depicted in Fig. 6, which shows the diameter and CARS signal as a function of time after immersion of the hair in water. The hair diameter is seen to expand by 15% (volume increasing by 31%) within 2.5 min after application of water. The CARS water signal increase follows the same temporal trend as the expansion of the hair. Note that in this dynamic measurement, the CARS intensity is monitored rather than the ratiometric signal. Although the relative CARS intensity is not a direct measure of the water concentration, it provides clear evidence for the direct temporal correlation between the water increase and the swelling of the hair fiber. After 2.5 min, the increase of the CARS signal in the cortex subsides, while the water signal measured in the medulla continues to rise. The different trend in water uptake between the cortex and the medulla is reproducible ($n=3$) and indicates that saturation of water absorption in the keratin-dense cortex is reached before the maximum water concentration is attained in the medulla.

3.4 *Uptake of Glycine by the Hair*

Glycine is a small molecule of direct relevance to hair cosmetic products, yet its absorption by the hair and the subsequent distribution of the chemical in the cortex on a micrometer scale has hitherto not been characterized. Glycine has a Raman spectrum with insufficient spectral specificity for a proper discrimination in the hair matrix using CARS microscopy. However, spectral selectivity can be attained by using deuterated glycine. When fivefold deuterated d-glycine is dissolved in water, three of the substituted deuterium atoms readily exchange with hydrogen at the amido and hydroxy groups. Glycine remains deuterated at the CD_2 group in aqueous solution, and the single CD_2 unit of the molecule exhibits a unique spectral Raman signature with limited overlap from the vibrational response of endogenous hair components.

The CARS spectrum of a d-glycine crystal in the CD_2 stretching vibration range is given in Fig. 7. Two clear peaks can be recognized, corresponding to the symmetric (2145 cm^{-1}) and asymmetric (2248 cm^{-1}) stretching vibration of the CD_2 unit. Upon dilution in water, these signatures can still be resolved, albeit at reduced contrast due to the relatively large contribution of the water nonresonant background. To improve contrast, the ratio between 2140 and 2160 cm^{-1} is taken as a measure for the presence of d-glycine. Figure 8 shows how the ratio signal scales with the concentration of d-glycine in water. A linear relation is found. Following Eq. (1), this linear dependence is expected for a

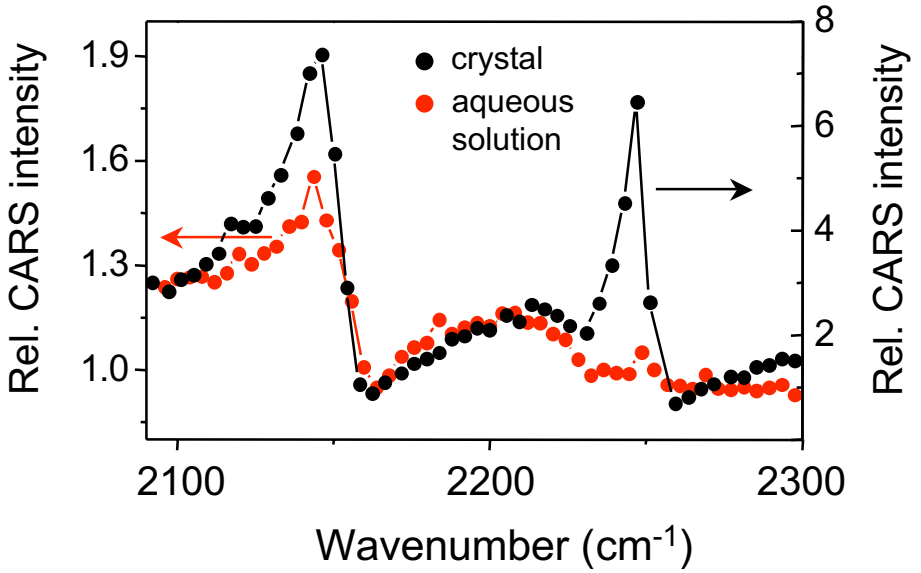

Fig. 7 CARS spectra of d-glycine in the CD_2 stretching region. Black dots indicate the spectrum obtained from a d-glycine crystal, whereas red dots represent the spectrum of a saturated aqueous d-glycine solution (3.3 M). CARS signals are measured relative to the nonresonant response of a glass coverslip. (Color online only.)

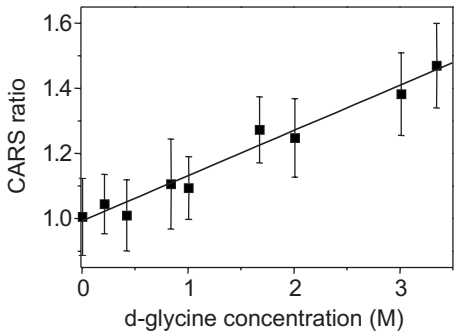

Fig. 8 Dependence of the CARS ratio signal (2140 cm^{-1}/2160 cm^{-1}) as a function of d-glycine concentration in an aqueous solution.

weak Raman scatterer. The different concentration dependence of the ratiometric signal for d-glycine compared to water (Fig. 4) is largely due to the difference in the relative strength of the vibrationally resonant contribution of these different molecular agents.

Figure 9 depicts d-glycine concentration maps obtained from ratio images in combination with the calibration curve of Fig. 8. When the hair fiber is immersed in a saturated solution of d-glycine, a significant fraction of the compound can be found inside the hair. It is seen that the distribution of d-glycine throughout the hair is virtually homogeneous. The concentration map shows that the d-glycine concentration outside the hair is 3.3 M, which corresponds to the expected concentration for a saturated solution. In the cortical regions of the hair, the average d-glycine concentration was found to be 0.22 ± 0.08 M ($n=3$). We found that the concentration varied from hair to hair. To test the accuracy of the d-glycine measurements, we have also performed reference measurements (at the d-glycine resonances) in a water immersed hair, showing a background contrast of 0.08 ± 0.16 M ($n=3$) in the cortex. The difference between the d-glycine measurement and the background reference is evident, indicating that the concentration contrast observed in the hair fiber, as shown in Fig. 9, can be attributed to the presence of d-glycine.

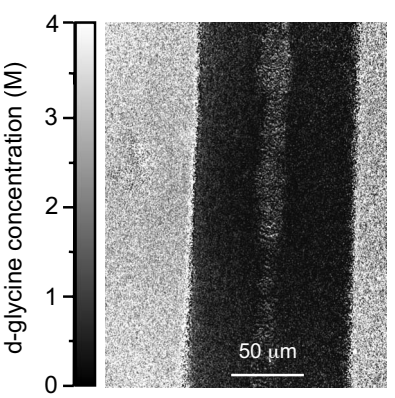

Fig. 9 D-glycine concentration map of a hair immersed in a saturated solution of d-glycine, as determined from CARS ratio images (2140 cm^{-1}/2160 cm^{-1}). The concentration outside the hair is 3.3 M and the average concentration in the cortical regions of the hair is 0.22 ± 0.08 M.

4 Discussion

The aim of this study is to determine the usefulness of CARS microscopy for hair research. We have applied this visualization technique to highlight endogenous structures in the hair and to quantitatively detect the concentration and distribution of externally applied molecular agents. In particular, we have applied a ratiometric procedure that enables a full retrieval of the concentration of molecular compounds in the strongly scattering hair fiber.

Our study reveals that CARS microscopy allows for a visual separation of endogenous components of the hair. The integrated CARS spectrum of the whole hair contains the same spectral information as previously published Raman spectra in the 2800–3000 cm^{-1} range.[12] Compared to previous Raman studies, the CARS approach taken here is much more conducible for imaging the spatial location of different components. In particular, the heterogeneous distribution of lipid-rich clusters in the medulla resolved in this work provides a possible explanation for the globular regions previously observed in structural SEM studies.

The strength of the vibrational CARS signal is dependent on the amount of the Raman active substance in the focal volume. Hence, a careful signal analysis or a comparison to a calibration curve can be used to retrieve the concentration of a compound in each pixel. Such quantitative approaches have proved useful when analyzing the concentration of lipid components in membranes[27] and adipocytes.[28] Compared to the CARS signal from lipids, quantitative imaging of d-glycine in hair is challenging because of the intrinsically small response from a single CD_2 oscillator per glycine molecule. In addition, hair has a highly scattering, complex architecture, which reduces the overall signal yield even further.

To verify the feasibility of the CARS methodology to quantitatively image the concentration of a small molecule, such as glycine in hair, we have first performed measurements on water, a well-characterized substance in the hair. On the basis of the CARS ratio images, the estimated concentration of water in hair at full hydration is 34%, which is in excellent agreement with the expected water concentration. We conclude that the CARS ratio method provides a reliable estimate of the actual concentration of the vibrationally resonant compound in a highly scattering medium such as hair.

We have used saturated solutions of d-glycine to maximize the concentration of the target compound in the hair. The concentration maps in the hair indicate that under such conditions d-glycine is present in the hair at fairly high concentrations. Because of the intrinsically low CARS signal yield from d-glycine, we have preformed control measurements in water under similar conditions to verify whether the contrast observed can be solely attributed to the presence of the compound. The control measurements indicated that such contrast assignment is indeed warranted in the cortex, where signal variation is minor due to relatively constant scattering properties in this region. However, near areas of significant refractive index changes, such as near the hair surface and the medulla/cortex interface, the ratio signal is affected by the low CARS signal detected from these strongly scattering regions. Low signal yields in scattering regions correspond to low signal to noise in the ratio images. To maximize accuracy, the glycine concentration was determined only in the cortical

regions away from the medulla. Under these conditions, the quantitative analysis shows that the CARS ratiometric method is capable of reliably detecting the presence of d-glycine in the hair. This observation is encouraging and sets the stage for the measurement of other chemical agents that are present at a lower concentration in the hair.

5 Conclusion

In this work, we have shown that CARS microscopy enables the detection of small molecules in intact human hair fibers. In addition, we have demonstrated that high-resolution molecular concentration maps can be generated in highly scattering media using CARS ratiometric imaging. On the basis of this methodology, we determined that the water concentration in fully hydrated hairs amounts to 34% by volume, in close agreement with previously reported values in literature. In addition, CARS imaging was shown to exhibit sufficient sensitivity to detect the presence of d-glycine in hair fibers. Our measurements show that externally applied d-glycine homogeneously distributes throughout the hair at concentrations of ~0.2 M. The ability to measure the penetration of small molecules such as water and glycine inside the hair without the requirement of either fluorescent labels or significant sample preparation is a significant advancement to the study of hair science. It is of direct relevance to evaluating the interaction of small molecules with the hair and the correlation between the agent penetration and the impact of the agent on product performance.

Acknowledgments

This work was funded by The Procter & Gamble Company. Equipment support was obtained from the National Science Foundation, Grant No. DBI-0754624. We thank Tiffany Valenton for assistance in some of the experiments.

References

1. C. J. S. M. Silva, A. Vasconcelos, and A. Caraco-Paulo, "Peptide structure: its effect on penetration into human hair," *Int. J. Cosmet. Sci.* **58**, 339–346 (2007).
2. C. R. Robbins, *Chemical and Physical Behavior of Human Hair*, 3rd ed., pp. 233–261, Springer Verlag, New York (1994).
3. M. S. C. Birbeck and E. H. Mercer, "The electron microscopy of the human hair follicle. Part II: the hair cuticle," *J. Biophys. Biochem. Cytol.* **3**, 215–221 (1957).
4. R. C. C. Wagner, P. K. Kiyohara, M. Silveira, and I. Joekes, "Electron microscope observations of human hair medulla," *J. Microsc.* **226**, 54–63 (2007).
5. J. M. Lagarde, P. Peyre, D. Redoules, D. Black, M. Briot, and Y. Gall, "Confocal microscopy of hair," *Cell Biol. Toxicol.* **10**, 301–304 (1994).
6. F. Formanek, Y. D. Wilde, G. S. Luengo, and B. Querleux, "Investigation of dyed human ahir fibres using apertureless near-field scanning optical microscopy," *J. Microsc.* **224**, 197–202 (2006).
7. C. Collin, B. Gautier, O. Gaillard, P. Hallegot, S. Chabane, P. Bastien, M. Payton, M. Bouleau, S. Thibaut, F. Pruche, A. Duranton, and B. A. Bernard, "Protective effects of taurine on human hair follicle grown *in-vitro*," *Int. J. Cosmet. Sci.* **28**, 289–298 (2006).
8. F. K. Wortmann, M. Gotsche, and H. Schmidt-Lewerkühne, "Diffusion and distribution of element-labelled surfactants in human hair," *Int. J. Cosmet. Sci.* **26**, 61–69 (2004).
9. A. Kelch, S. Wessel, T. Will, U. Hintze, R. Wepf, and R. Wiesendanger, "Penetration pathways of fluorescent dyes in human hair fibers investigated by scanning near-field optical microscopy," *J. Microsc.* **200**, 179–186 (2000).
10. P. Corcuff, P. Gremillet, M. Jourlin, Y. Duvault, F. Leroy, and J. L. Leveque, "3D reconstruction of human hair by confocal microscopy," *J. Soc. Cosmet. Chem.* **44**, 1–12 (1993).
11. J. L. Bantignies, F. Fuchs, G. L. Carr, G. P. Williams, D. Lutz, and S. Marull, "Organic reagent interaction with hair spatially characterized by infrared microspectroscopy using synchrotron radiation," *Int. J. Cosmet. Sci.* **20**, 381–394 (1998).
12. A. C. Williams, H. G. M. Edwards, and B. W. Barry, "Raman spectra of human keratotic biopolymers: skin, callus, hair and nail," *J. Raman Spectrosc.* **25**, 95–98 (1994).
13. J. X. Cheng, "Coherent anti-Stokes Raman scattering microscopy," *Appl. Spectrosc.* **91**, 197–208 (2007).
14. C. L. Evans and X. S. Xie, "Coherent anti-Stokes Raman scattering microscopy: chemical imaging for biology and medicine," *Annu. Rev. Anal. Chem.* **1**, 883–909 (2008).
15. C. W. Freudiger, W. Min, B. G. Saar, S. Lu, G. R. Holtom, C. He, J. C. Tsai, J. X. Kang, and X. S. Xie, "Label-free biomedical imaging with high sensitivity by stimulated Raman scattering microscopy," *Science* **322**, 1857–1861 (2008).
16. T. B. Huff, Y. Shi, Y. Yan, H. Wang, and J. X. Cheng, "Multimodel nonlinear optical microscopy and applications to central nervous system," *IEEE J. Sel. Top. Quantum Electron.* **14**, 4–9 (2008).
17. T. T. Le, I. M. Langohr, M. J. Locker, M. Sturek, and J. X. Cheng, "Label-free molecular imaging of atherosclerotic lesions using multimodal nonlinear optical microscopy," *J. Biomed. Opt.* **12**, 054007 (2007).
18. T. Gao, "Evaluation of hair humidity resistance/moisturization from hair elasticity," *Int. J. Cosmet. Sci.* **58**, 393–404 (2007).
19. J. Marsh, R. M. Dahlgren, C. Clarke, J. Stonehouse, and C. Nunn, "A new oxidant for hair coloring," *Int. J. Cosmet. Sci.* In press (2009).
20. W. S. Rasband, *Image J. Nurs. Sch.* National Institutes of Health, Bethesda (1997–2009).
21. F. Ganikhanov, C. L. Evans, B. G. Saar, and X. S. Xie, "High-sensitivity vibrational imaging with frequency modulation coherent anti-Stokes Raman scattering (FM-CARS) microscopy," *Opt. Lett.* **31**, 1872–1874 (2006).
22. O. Burkacky, A. Zumbusch, C. Brackmann, and A. Enejder, "Dual-pump coherent anti-Stokes Raman scattering microscopy," *Opt. Lett.* **31**, 3656–3658 (2006).
23. L. Kreplak, F. Briki, Y. Duvault, J. Doucet, C. Merigoux, F. Leroy, L. Lévêque, L. Miller, G. L. Carr, G. P. Williams, and P. Dumas, "Profiling lipids across Caucasian and Afro-American hair transverse cuts, using synchrontron infrared microspectroscopy," *Int. J. Cosmet. Sci.* **23**, 368–374 (2001).
24. H. W. Wang, T. T. Le, and J. X. Cheng, "Label-free imaging of arterial cells and extracellular matrix using a multimodal CARS microscope," *Opt. Commun.* **281**, 1813–1822 (2008).
25. C. Bouillon and J. Wilkinson, *The Science of Hair Care*, Informa Healthcare, London (2005).
26. P. B. Stam, R. F. Kratz, and H. J. White, "The swelling of human hair in water and water vapor," *Text. Res. J.* **22**, 448–465 (1952).
27. L. Li, H. Wang, and J. X. Cheng, "Quantitative coherent anti-Stokes Raman scattering imaging of lipid distribution in coexisting domains," *Biophys. J.* **89**, 3480–3490 (2005).
28. H. A. Rinia, K. N. J. Burder, M. Bonn, and M. Müller, "Quantitative label-free imaging of lipid composition and packing of individual cellular lipid droplets using multiplex CARS microscopy," *Biophys. J.* **95**, 4908–4914 (2008).